Colloids and Surfaces B: Biointerfaces 113 (2014) 302–311

Contents lists available at ScienceDirect

Colloids and Surfaces B: Biointerfaces

journal homepage: www.elsevier.com/locate/colsurfb

In situ preparation of magnetic Fe_3O_4 nanoparticles inside nanoporous poly(L-glutamic acid)/chitosan microcapsules for drug delivery

Shifeng Yan [a,*], Xin Zhang [a], Yuanyuan Sun [a], Taotao Wang [a], Xuesi Chen [b,*], Jingbo Yin [a,*]

[a] Department of Polymer Materials, Shanghai University, Shanghai 200444, China
[b] Key Laboratory of Polymer Ecomaterials, Changchun Institute of Applied Chemistry, Chinese Academy of Sciences, Changchun 130022, China

ARTICLE INFO

Article history:
Received 22 July 2013
Received in revised form 27 August 2013
Accepted 3 September 2013
Available online xxx

Keywords:
Magnetic microcapsules
Fe_3O_4 nanoparticles
Nanoporous microcapsules

ABSTRACT

The magnetic polymer microcapsules, as a promising environmental stimuli-responsive delivery vehicle, have been increasingly exploited to tackle the problem of remotely navigated delivery. This study presented a novel design and fabrication of magnetic poly(L-glutamic acid)/chitosan (PGA/CS) microcapsules. Magnetic Fe_3O_4 nanoparticles were in situ synthesized inside nanoporous PGA/CS microcapsules and resultant magnetic PGA/CS microcapsules were characterized. Mitoxantrone (MTX), an antineoplastic drug, was chosen as a water-soluble model drug to research the loading and release properties of the microcapsules. The results showed the carboxylate groups of PGA within polyelectrolyte walls could be used as binding sites for the absorption of iron ions and reaction sites for the synthesis of magnetic nanoparticles. Magnetic PGA/CS microcapsules were dissected using a dual-beam scanning electron microscope/focused ion beam (SEM/FIB) for morphological and microstructural examination. It was found that Fe_3O_4 nanoparticles with size of about 10 nm were homogeneously dispersed in the polymer matrix and adhered to the pore walls of the microcapsules. Increasing the concentration of iron ions led to an increasing loading content of Fe_3O_4 nanoparticles and an increase in the resultant magnetization. The magnetic PGA/CS microcapsules could be easily manipulated by an external magnetic field. The MTX loading capacity depended on loading time and MTX concentration. The high loading could be ascribed to spontaneous deposition of MTX induced by electrostatic interaction. The microcapsules exhibited sustained release behavior. The MTX release from microcapsules could be best described using Korsmeyer–Peppas and Baker–Lonsdale models, indicating the diffusion mechanism of drug release from both PGA/CS microcapsules and magnetic PGA/CS microcapsules. Therefore, the novel magnetic PGA/CS microcapsules are expected to find application in drug delivery systems because of the properties of magnetic sensitivity, high drug loading and sustained release.

1. Introduction

Environmental stimuli-responsive microcapsules have found many applications in various fields, including drug delivery, biosensoring, electrocatalysis, and enzyme immobilization [1], owing to the small size, large inner volume, tunable permeability, and especially the control release of their contents in response to external environmental stimuli, such as changes of temperature, pH, ion, magnetic field, electric field, etc. [2–6].

The magnetic polymer microcapsules, as a promising environmental stimuli-responsive delivery vehicle, have been increasingly exploited to tackle the problem of remotely navigated delivery. The magnetic polymer microcapsules also exhibit the multi-functional therapeutic advantages of controlled drug delivery and thermal therapy (hyperthermia cancer treatment). The reported routes for preparation of magnetic microcapsules mainly focused on emulsion polymerization [7] and suspension polymerization [8–10] in the presence of magnetic nanoparticles, which often resulted in aggregation of magnetic nanoparticles.

The layer-by-layer (LbL) assembled polyelectrolyte microcapsules have attracted particular interest because of their tailored properties, such as size, composition, surface functionality and so on [11,12], and find potential applications in medicine, drug delivery, micro-reactor, catalysis, etc. [13–15]. However, in the application of drug delivery system, the drug loadings achieved are typically low, as the maximum concentration of drug inside the capsules is often limited to the concentration in the solution [16].

A common way to endow the polyelectrolyte multilayer microcapsules with magnetic properties is the introduction of preformed magnetic nanoparticles. The microcapsules might be applied as microscale containers for loading of magnetic nanoparticles by

* Corresponding authors. Tel.: +86 2166138055.
E-mail addresses: yansf@staff.shu.edu.cn (S. Yan), xschen@ciac.jl.cn (X. Chen), jbyin@oa.shu.edu.cn (J. Yin).

0927-7765/$ – see front matter © 2013 Elsevier B.V. All rights reserved.
http://dx.doi.org/10.1016/j.colsurfb.2013.09.004

permeability regulation [17]. Also, the microcapsules could be fabricated via alternate electrostatic adsorption between magnetic nanoparticles and opposite charged polyelectrolytes [18]. However, the incorporation of preformed magnetic nanoparticles often resulted in aggregation of nanoparticles. Alternatively, the in situ preparation of magnetic nanoparticles inside hollow polyelectrolyte microcapsules utilizing a pH gradient across the capsule shell was reported by Shchukin et al. [19]. Still these magnetic nanoparticles were liable to aggregate. And the obtained magnetic nanoparticles were mixed with traces of nonmagnetic metal oxides and γ-Fe_2O_3.

In our previous work, nanoporous multilayer poly(L-glutamic acid)/chitosan (PGA/CS) microcapsules were fabricated by LbL assembly using the porous silica particles as sacrificial templates. Nanoporous microcapsules with internal support of polyelectrolyte network and high surface area ensure their properties of good structural stability and high drug loading capability [20].

In this paper, we demonstrate the in situ synthesis of magnetic nanoparticles using the nanoporous PGA/CS microcapsules as the microreactors. Compared with the hollow LbL microcapsules, the nanoporous microcapsules with high surface area provide more reaction sites for the synthesis of magnetic nanoparticles and are expected to reduce the particle aggregation. Mitoxantrone (MTX), an antineoplastic drug, was used as model water-soluble drug to research the loading and release properties of the magnetic microcapsules. To the best of our knowledge, this is the first study of the in situ synthesis of magnetic nanoparticles in nanoporous LbL microcapsules, accompanied by the demonstration of drug loading and release properties of the magnetic hybrid systems.

2. Experimental

2.1. Materials

Poly(L-glutamic acid) ($M_v = 4.0 \times 10^4$) was prepared from poly(γ-benzyl-L-glutamate) (PBLG), which was synthesized by the ring opening polymerization of the *N*-carboxyanhydride (NCA) of γ-benzyl-L-glutamate in our laboratory [21]. CS ($M_v = 4.0 \times 10^4$) was purchased from Jinan Haidebei Marine Bioengineering Corp. (Shandong, China). 1-Ethyl-3-(3-dimethylaminopropyl) carbodiimide hydrochloride (EDC) was purchased from Covalent Chemical Technology Co., Ltd. (Shanghai, China). Mitoxantrone (MTX) was purchased from Beijing Shilian Hengtong Chemical Technology Co., Ltd. (Beijing, China). Other reagents were all analytical grade and used as received.

2.2. In situ synthesis of magnetic PGA/CS microcapsules

Nanoporous PGA/CS microcapsules were prepared by LbL assembly of PGA and CS using the porous silica particles as sacrificial templates, as reported previously by us [20]. The preparation of magnetite (Fe_3O_4) nanoparticles within PGA/CS microcapsules was carried out as follows: at first, 1 mg of PGA/CS microcapsules were immersed in 4 mL of $FeSO_4/Fe_2(SO_4)_3$ solution for 4 h to allow iron ions to be absorbed to the carboxylate groups of PGA in the polyelectrolyte walls. The Fe^{2+}/Fe^{3+} molar ratio was set at 1:2 and Fe^{3+} concentration ranged from 0.4 to 1.6 mol/L. The system was purged with N_2. Excess iron ions were removed by centrifugation (12,000 rpm, 3 min) and washing with deionized water. Then the Fe^{2+}/Fe^{3+} contained PGA/CS microcapsules were dispersed in 4 mL of deionized water, 1 mol/L NaOH aqueous solution was slowly added until pH 9 was achieved. The color of the dispersion turned to brown after 5 h. The resultant magnetic PGA/CS microcapsules were obtained after three centrifugation/washing cycles (as above) and subsequent freeze-drying for 48 h.

The schematic illustration of the procedure used in the fabrication of magnetic PGA/CS microcapsules was shown in Fig. 1.

2.3. MTX loading and release

1 mg of magnetic PGA/CS microcapsules were dispersed in 5 mL of MTX aqueous solution for absorption. In order to study the effect of loading time on the loading capacity of magnetic microcapsules, the microcapsules were incubated in MTX solution of 0.5 mg/mL for 1–6 h. As for the drug concentration dependent experiment, the loading time was set at 4 h, while the concentration of MTX solution varied from 0.1 to 1.0 mg/mL. After being incubated under various conditions, the MTX-loaded microcapsules were centrifuged (12,000 rpm, 3 min), washed for 2 times with de-ionized water and freeze-dried for further use in release experiments.

The concentration of MTX remained in the supernatant after centrifugation was measured at 609 nm wavelength, which was the UV–vis spectroscopy characteristic absorption wavelength. The MTX loading inside the microcapsules was calculated from the change of MTX concentrations in the supernatant. All the data were averaged from 3 parallel experiments.

For the examination of MTX release, 5 mg of MTX-loaded magnetic microcapsules were carefully enveloped into dialysis bags and exposed to 100 mL phosphate buffer solution (PBS) (pH 7.4). 5 mL buffer solution was fetched from release system with reconstitution of 5 mL fresh buffer solution at every predetermined time. The concentration of the MTX released from this drug delivery system was monitored at 609 nm of UV absorbance.

For comparison, the drug loading and release experiment of PGA/CS microcapsules were conducted.

2.4. Characterization methods

Zeta (ζ) potentials were determined with Malvern Zetasizer 3000HS equipped with MPT-1 titrator (Malvern, Worcestershire, UK). Electrophoretic mobilities were converted to ζ-potentials using Smoluchowski's equation.

The FTIR spectra were recorded using a FT-IR spectrophotometer (AVATAR 370, Nicolet, USA) in the region of 4000–500 cm^{-1}.

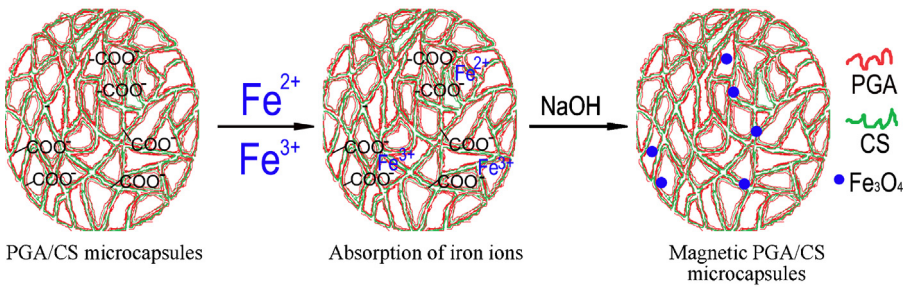

Fig. 1. Schematic illustration for the preparation of magnetic PGA/CS microcapsules.

The X-ray photoelectron spectra (XPS) characterization was carried out on a photoelectron spectrometer (JEOL Ltd., ESCALABMKII) using Mg Kα radiation at 12 kV and 10 mA.

X-ray diffraction patterns were analyzed using a diffractometer (D/MAX2550, Rigaku, with Cu Kα radiation at a voltage of 40 kV and 30 mA. The samples were scanned between $2\theta = 5–40^\circ$ with a scanning speed of 5°/min. Prior to testing, the samples were dried and stored in a desiccator.

Scanning electron microscopy (SEM, JEOL, JSM-6700F) was used to examine the morphologies of the samples. Samples for SEM observation were prepared by depositing suspensions of microcapsules on Si slides.

To image the cross-section and analyze the internal microstructure of the magnetic nanoporous PGA/CS microcapsules, an in situ dual-beam microscope (Scanning Electron Microscope and Focused Ion Beam, also called SEM–FIB), FEI Helios NanoLab 650 consisting of a standard ion column which allows Ga^+ cleaning and milling in a range of 500 V–30 kV, was utilized. Carbon glue was used to effectively attach the specimen to the stub in order to reduce specimen drifts. To increase the sample's conductivity during SEM imaging and protect the sample from ion damage, protective platinum layers were deposited with an in situ liquid metal-organic ion source (LMIS).

UV–vis spectra were recorded on an Agilent 8453 UV–vis spectrophotometer.

TGA experiments were conducted using Simultaneous Thermal Analysis (STA409PC). The samples were heated from 25 to 600 °C with a heating rate of 10 °C/min under nitrogen flow.

Confocal micrographs of microcapsule samples were taken with an LSM700 confocal laser scanning microscopy (CLSM) (Carl Zeiss Inc.).

3. Results and discussion

3.1. Formation and structure of magnetic PGA/CS microcapsules

As mentioned above, Fe_3O_4 nanoparticles were in situ synthesized using the nanoporous PGA/CS microcapsules as microreactors. The carboxylate groups of PGA within polyelectrolyte walls could be used as binding sites for the absorption of iron ions and reaction sites for the synthesis of Fe_3O_4 nanoparticles [22]. The procedure in the fabrication of magnetic PGA/CS microcapsules was followed by microelectrophoresis, as shown in Fig. 2(a). PGA/CS microcapsules with outermost layer of PGA possessed negative charge because some carboxylate groups ionized in aqueous solution. The attachment of positive charged iron ions caused a

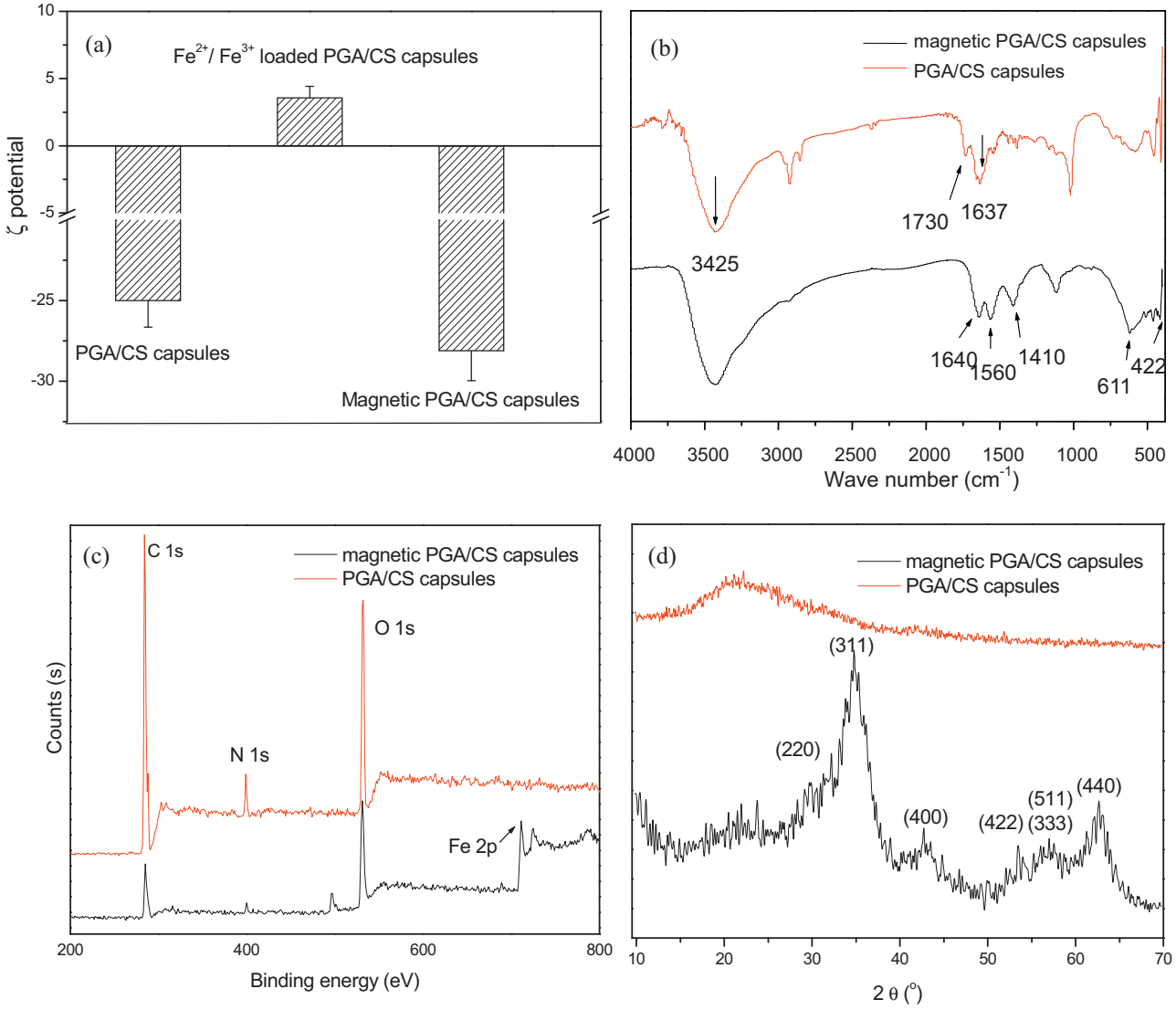

Fig. 2. In situ fabrication of magnetic PGA/CS microcapsules. (a) Variation of ζ-potential during the preparation of magnetic PGA/CS microcapsules, (b) XPS spectra, (c) FTIR spectra and (d) X-ray diffraction patterns of PGA/CS microcapsules and magnetic PGA/CS microcapsules.

reversal in the ζ-potential to approximately 3.6 mV. After addition of NaOH aqueous solution, magnetic nanoparticles were in situ synthesized via the co-precipitation of iron ions (Fe^{2+}/Fe^{3+} = 1:2), the ζ-potential of resultant magnetic PGA/CS microcapsules decreased drastically from 3.6 to −28 mV. It was reported that isoelectric point (p*I*) of Fe_3O_4 nanoparticles synthesized by the co-precipitation of Fe^{2+} and Fe^{3+} ions in aqueous ammonia solution shifted from 6.78 to 2.64 after polyacrylic acid (PAA) binding [23], revealing negative charge of Fe_3O_4 nanoparticles under neutral pH conditions and increase of negative charge density after functionalization with polyanion. Similar to the aforementioned result, for magnetic PGA/CS microcapsules, the ζ-potentials of −28 mV could be ascribed to the negative charge from magnetic nanoparticles and exposed carboxylate groups of PGA within polyelectrolyte walls of the microcapsules.

Fig. 2(b) presented the FTIR spectra of PGA/CS microcapsules before and after Fe_3O_4 loading. For PGA/CS microcapsules, the absorption bands at 1637 and 1730 cm^{-1} originated from C=O and amide I groups, respectively [24]. With respect to magnetic PGA/CS microcapsules, the absorption bands at 422 and 611 cm^{-1} were ascribed to Fe—O bending vibrations of the incorporated Fe_3O_4 [25,26]. The original characteristic absorptions at 1637 and 1730 cm^{-1} almost disappeared, new absorption bands appeared at peaks of 1560 and 1640 cm^{-1}, which means strong interaction between PGA/CS microcapsules and Fe_3O_4 nanoparticles. Strong interaction between in situ synthesized Fe_3O_4 nanoparticles and the cellulose matrix microspheres was also confirmed by peak wavelength shifts in the FTIR spectrum [27].

XPS was applied to provide elemental information of surface composition of PGA/CS microcapsules before and after Fe_3O_4 loading, as shown in Fig. 2(c). The C1s, N1s and O1s peaks of PGA/CS microcapsules located at 530.9, 532.35, and 532.6 eV, respectively [28]. For magnetic PGA/CS microcapsules, a new peak was detected at 707 eV, which could be ascribed to Fe 2p peak [29]. There were C, N, O and Fe elements in the composite magnetic microcapsules, which further proved that Fe_3O_4 nanoparticles had been in situ synthesized in the PGA/CS microcapsules.

Fig. 2(d) showed the X-ray diffraction patterns of PGA/CS microcapsules before and after Fe_3O_4 loading. For PGA/CS microcapsules, only a broad peak centered at 21.6° was observed, corresponding to the amorphous nature. For magnetic PGA/CS microcapsules, it was clear that the Fe_3O_4 phase exhibited a higher crystallinity than that of amorphous PGA/CS matrix. The X-ray diffraction pattern displayed some distinct peaks at 30.14°, 35.40°, 43.38°, 53.54°, 57.04° and 62.58°, respectively, assigned to (2 2 0), (3 1 1), (4 0 0), (4 2 2), (5 1 1/3 3 3) and (4 4 0) planes of the spinel structured Fe_3O_4 phase according to the standard ICDD PDF (Card No. 88-1436) [30]. It was also one of the evidences that Fe_3O_4 had been successfully loaded into the PGA/CS microcapsules.

Morphology observation of PGA/CS microcapsules before and after Fe_3O_4 loading was conducted using SEM, as shown in Fig. 3. The PGA/CS microcapsules had a rough surface with an average diameter of about 2 μm, as shown in Fig. 3(a). PGA/CS magnetic microcapsules retained the original shape of PGA/CS microcapsules with no sign of rupture or collapse, as shown in Fig. 3(b). In order to investigate the inner structure of the samples, the frozen microcapsules were grinded with liquid nitrogen using mortar and pestle. Fig. 3(c) and (d) showed the morphology of the broken samples. Compared with PGA/CS microcapsules, magnetic PGA/CS microcapsules exhibited rougher fracture surface.

The SEM–FIB dual beam microscope is capable of standard SEM viewing and FIB milling to remove sections of the sample surface to a specified height, depth and width, which is precise enough to be used for ultramicrotomy [31]. FIB allows particles to be dissected, while preserving pores and interfacial voids that would otherwise be destroyed by conventional, mechanical polishing [32]. In this study, slice-and-view (FIB/SEM) was used to further study the inner microstructure of magnetic PGA/CS microcapsules, as shown in Fig. 3(e). Nanoporous structure of magnetic PGA/CS microcapsules was clearly seen in the cross-section made by milling with the Ga^+ beam. Fe_3O_4 nanoparticles with the average size of about 10 nm were homogeneously dispersed in the polymer matrix (Fig. 3(e)-1) and adhered to the pore walls of the microcapsules (Fig. 3(e)-1) with no obvious agglomeration. It was further confirmed that Fe_3O_4 nanoparticles could be readily impregnated into the PGA/CS microcapsules. The uniform dispersion of magnetic nanoparticles could be ascribed to immobilization to the macromolecules via electrostatic interaction and the isolation by polyelectrolyte walls.

3.2. Control of Fe_3O_4 content and magnetic properties of resultant magnetic PGA/CS microcapsules

The magnetic microcapsules were fabricated from different concentrations of iron ion in order to control Fe_3O_4 content and magnetic properties.

Fig. 4(a) and (b) presented the X-ray diffraction patterns and the FTIR spectra of magnetic PGA/CS microcapsules fabricated from different concentrations of iron ion. The strength of the characteristic peaks of Fe_3O_4 increased gradually with Fe^{3+} concentration (Fe^{3+}/Fe^{2+} = 2), revealing the increasing Fe_3O_4 content at higher iron ions.

A more direct assay of the Fe_3O_4 content of magnetic PGA/CS microcapsules was provided by TGA. Thermodynamic behaviors of PGA/CS microcapsules before and after Fe_3O_4 loading were shown in Fig. 4(c). The degradations of PGA/CS microcapsules consisted of two stages, corresponding to evaporation of absorbed water and decomposition of polymer chains, respectively. Compared with PGA/CS microcapsules, the magnetic PGA/CS microcapsules presented relatively higher thermal degradation temperatures. These results suggested some possible interaction between PGA/CS microcapsules and incorporated Fe_3O_4 nanoparticles, thus enhancing the thermal stability of the composite microcapsules [33].

The Fe_3O_4 content could be estimated by the difference of remaining weight between magnetic PGA/CS microcapsules and PGA/CS microcapsules. The Fe_3O_4 content of magnetic PGA/CS microcapsules fabricated from different Fe^{3+} concentrations of 0.8, 1.0, 1.2 and 1.6 mol/L reached about 14.5, 19.5, 24.9 and 33.3 wt.%, respectively. Thus, the Fe_3O_4 content of the magnetic PGA/CS microcapsules could be simply adjusted by changing the iron ion concentration.

The average crystallite sizes of the incorporated Fe_3O_4 nanoparticles was estimated from the X-ray peak broadening of the (3 1 1) diffraction peak using Scherrer formula

$$D = \frac{k\lambda}{\beta \cos\theta}$$

where D is the average crystallite size, λ the X-ray wavelength (0.1542 nm), β the full-width at half-maximum (FWHM), θ the diffraction angle, and k a constant equal to 0.89 [34]. When the reflecting peak at $2\theta = 35.40°$ was chosen to calculate the average diameter, the average size of the Fe_3O_4 particles ranged from 8 to 10 nm, which was in accord with the result of FIB/SEM, as depicted in Fig. 3(e). The size of the Fe_3O_4 nanoparticles hardly changed with the increasing Fe_3O_4 content, which indicated that the microcapsules exerted a strong confinement effect on the growth of the Fe_3O_4 nanoparticles, similar phenomenon was also reported in the system of Fe_3O_4/cellulose microspheres [27].

Fig. 4(d) showed the hysteresis branches of the magnetization evolution as a function of the applied field. Almost no hysteresis was observed in these measurements, which was consistent with superparamagnetic properties of magnetic Fe_3O_4 nanoparticles with a

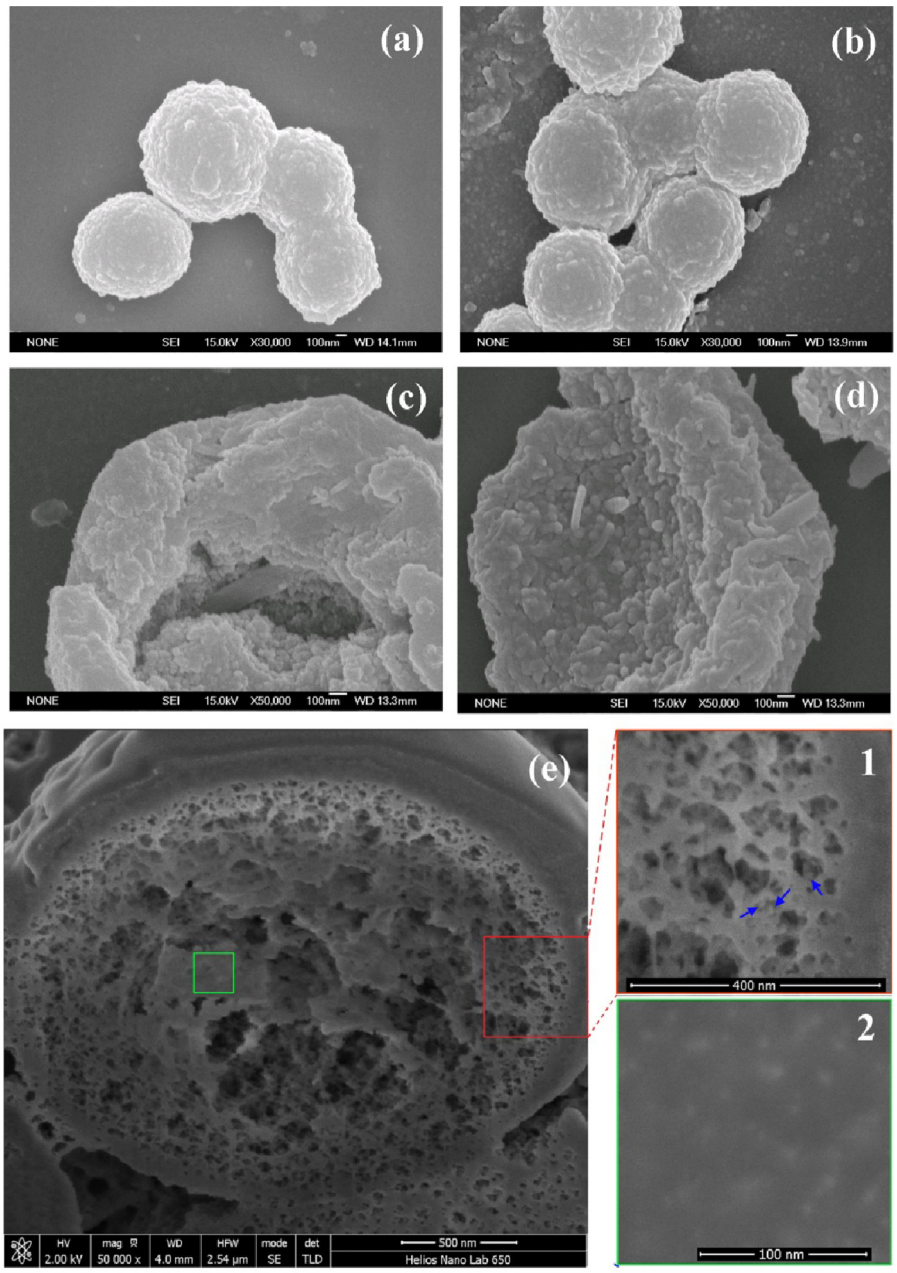

Fig. 3. Microstructure of microcapsules. SEM images of PGA/CS microcapsules (a, c) and magnetic PGA/CS microcapsules (b, d). (a and b) Intact samples, (c and d) broken samples; the cross-sectional view of magnetic PGA/CS microcapsules after FIB section and (e) higher magnification imaging of the cross-section (1–2).

diameter below 12 nm [35]. The magnetization did not reach saturation because of relatively low applied field, which also revealed small size of Fe_3O_4 nanoparticles [36]. Increasing iron ion concentration led to an increase in the magnetization, which could be ascribed to the increasing loading content of Fe_3O_4 nanoparticles.

Fig. 4(e) demonstrated the dispersion and separation process of the magnetic PGA/CS microcapsules. Without eternal magnetic field, magnetic PGA/CS microcapsules were brown in color and uniformly dispersed in water. Interestingly, when an external magnetic field was applied, the magnetic PGA/CS microcapsules could be easily attached to the sidewall from water solution. Therefore, the microcapsules possessed magnet-induced sensitivity, indicated the magnetic PGA/CS microcapsules could meet the requirement of magnetic drug targeting and be utilized as a potential targeting carrier in biomedical application.

3.3. *Interaction between MTX and magnetic PGA/CS microcapsules*

In order to elucidate the interaction between MTX and PGA/CS microcapsules, magnetic PGA/CS microcapsules before and after MTX loading were characterized.

The FTIR spectra of magnetic PGA/CS microcapsules with and without MTX loading were shown in Fig. 5(a). For comparison, the FTIR spectrum of MTX was also presented. In the spectrum of MTX, the characteristic peaks at 2930, 1565 and 1212 cm^{-1} were attributed to stretching vibration of $-CH_2$, C=O and phenolic hydroxyl groups, respectively. And the absorptions at 1607, 1517 and 1453 cm^{-1} were ascribed to aromatic nucleus [37]. All of these peaks existed in the spectrum of magnetic PGA/CS microcapsules with greatly reduced intensity. The above evidences indicated some

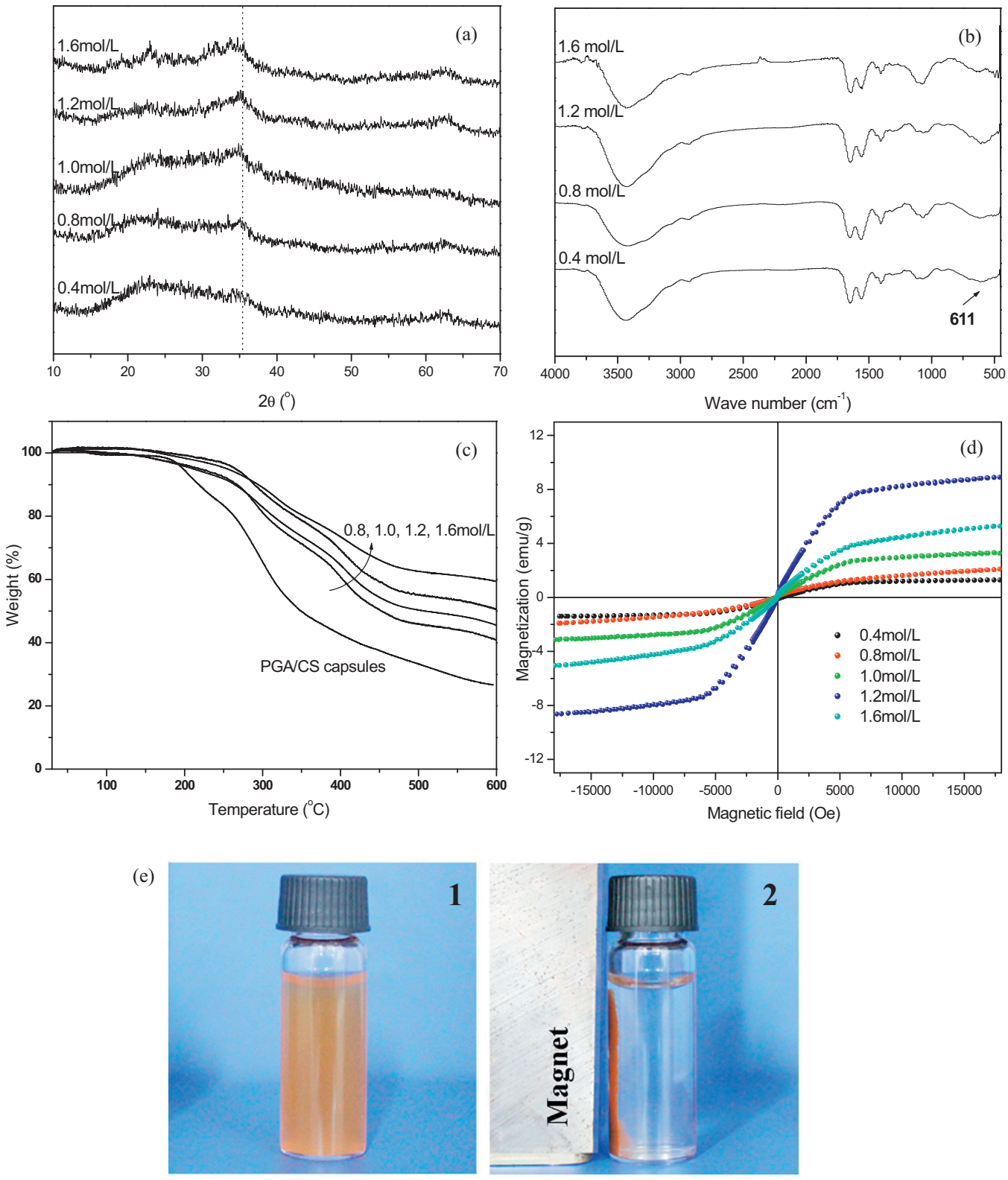

Fig. 4. Control of Fe_3O_4 content and magnetic properties of the magnetic PGA/CS microcapsules. (a) X-ray diffraction patterns, (b) FTIR spectra, (c) TGA curves and (d) magnetization curves of magnetic microcapsules fabricated from different Fe^{3+} concentration. (e) Digital photographs of the dispersion of magnetic PGA/CS microcapsules in the absence of external magnetic field (1) and separation with an external field (2).

interaction between MTX and PGA/CS microcapsules and substantially encapsulation of MTX in magnetic PGA/CS microcapsules.

Fig. 5(b) showed the X-ray diffraction patterns of bare MTX, magnetic PGA/CS microcapsules before and after MTX loading. Bare MTX presented highly crystalline nature, as illustrated by a strong characteristic peak at $2\theta = 26.2^\circ$ [38]. After encapsulation in magnetic PGA/CS microcapsules, no crystalline peaks of MTX were observed, revealing substantial loading of MTX and considerable

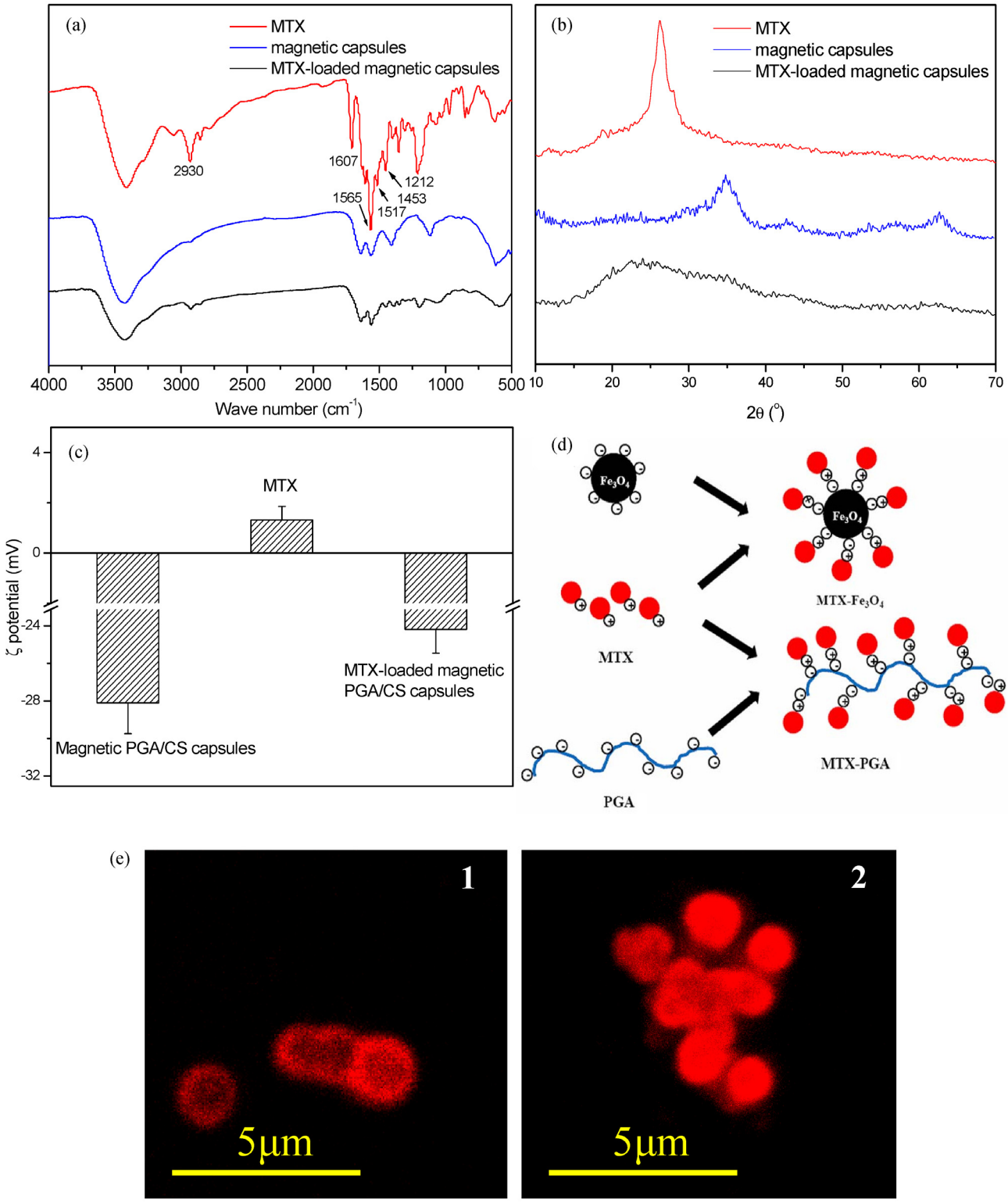

Fig. 5. Interaction between MTX and magnetic PGA/CS microcapsules. (a) FTIR spectra and (b) X-ray reflectivity of MTX, magnetic PGA/CS microcapsules before and after MTX loading. (c) Variation of ζ-potential of magnetic PGA/CS microcapsules during MTX loading. (d) Schematic representation of MTX bound to Fe_3O_4 nanoparticles and PGA chains. (e) CLSM image of MTX-loaded PGA/CS (1) and magnetic PGA/CS (2) microcapsules.

interaction between MTX and magnetic PGA/CS microcapsules. Amorphous nature of MTX was also found after loading in functionalized mesoporous silica nanoparticles (MSN) [38].

The main driving force for MTX loading in magnetic PGA/CS microcapsules could be ascribed to electrostatic interaction. The magnetic PGA/CS microcapsules were negatively charged with ζ-potential of −28 mV, which was due to carboxylate groups of PGA and negative charge characteristics of magnetic Fe_3O_4 nanoparticles. MTX bore positive charge with the ζ-potential of 1.3 mV because of positively charged nitrogen atoms from the lateral

chains of the drug [39]. After absorption of MTX, the ζ-potential changed to −24.2 mV because of partial neutralization of negative charge (Fig. 5(c)). The negatively charged Fe_3O_4 nanoparticles and outmost PGA chains could simultaneously adsorb MTX through electrostatic interaction, as displayed in Fig. 5(d).

Fig. 5(e) showed CLSM photographs of PGA/CS microcapsules and magnetic PGA/CS microcapsules after loading of MTX. Uniform fluorescence could be observed across the particle cross-sections due to the homogeneous distribution of MTX in the microcapsules. Compared with PGA/CS microcapsules, CLSM image of magnetic PGA/CS microcapsules showed increased fluorescence intensity, reflecting the higher drug loading. The incorporation of Fe_3O_4 nanoparticles facilitated MTX loading, which was ascribed to their electrostatic interaction with MTX.

3.4. MTX loading and release behavior

Fig. 6(a) shows the relationship between the MTX loading capacity and loading time in the MTX aqueous solution (0.5 mg/mL) under fixed microcapsule concentration. The loading capacity increased rapidly and reached the maximal value of 37.7% for magnetic PGA/CS microcapsules and 18.1% for PGA/CS microcapsules at 4 h, and then it decreased slightly and reached an equilibrate value. The MTX loading might be attributed to concentration difference and its electrostatic interaction with PGA and Fe_3O_4 nanoparticles, as discussed above.

In order to research the influence of MTX concentration on the drug loading capacity, the PGA/CS microcapsules were mixed with MTX solution with different concentrations. As shown in Fig. 6(b), when MTX concentration increased from 0.1 to 1.0 mg/mL, the drug loading content of magnetic PGA/CS microcapsules increased from 7.36% to 40.24%. As for PGA/CS microcapsules, this value increased from 3.38% to 25.12%.

The high loading and nonlinear increase of drug content with concentration could be attributed to the spontaneous deposition of water-soluble MTX into the magnetic PGA/CS microcapsules. Some positively charged substances have been reported to spontaneously accumulate inside the poly(styrenesulfonate)/poly(allylamine hydrochloride) (PSS/PAH) microcapsules with the driving force of electrostatic attraction between the incorporated positively charged substances and negatively charged PSS/melamine formaldehyde (MF) complex formed during the preparation of the microcapsules using MF microspheres as sacrificial templates [40,41]. Since MTX was positively charged, while magnetic PGA/CS

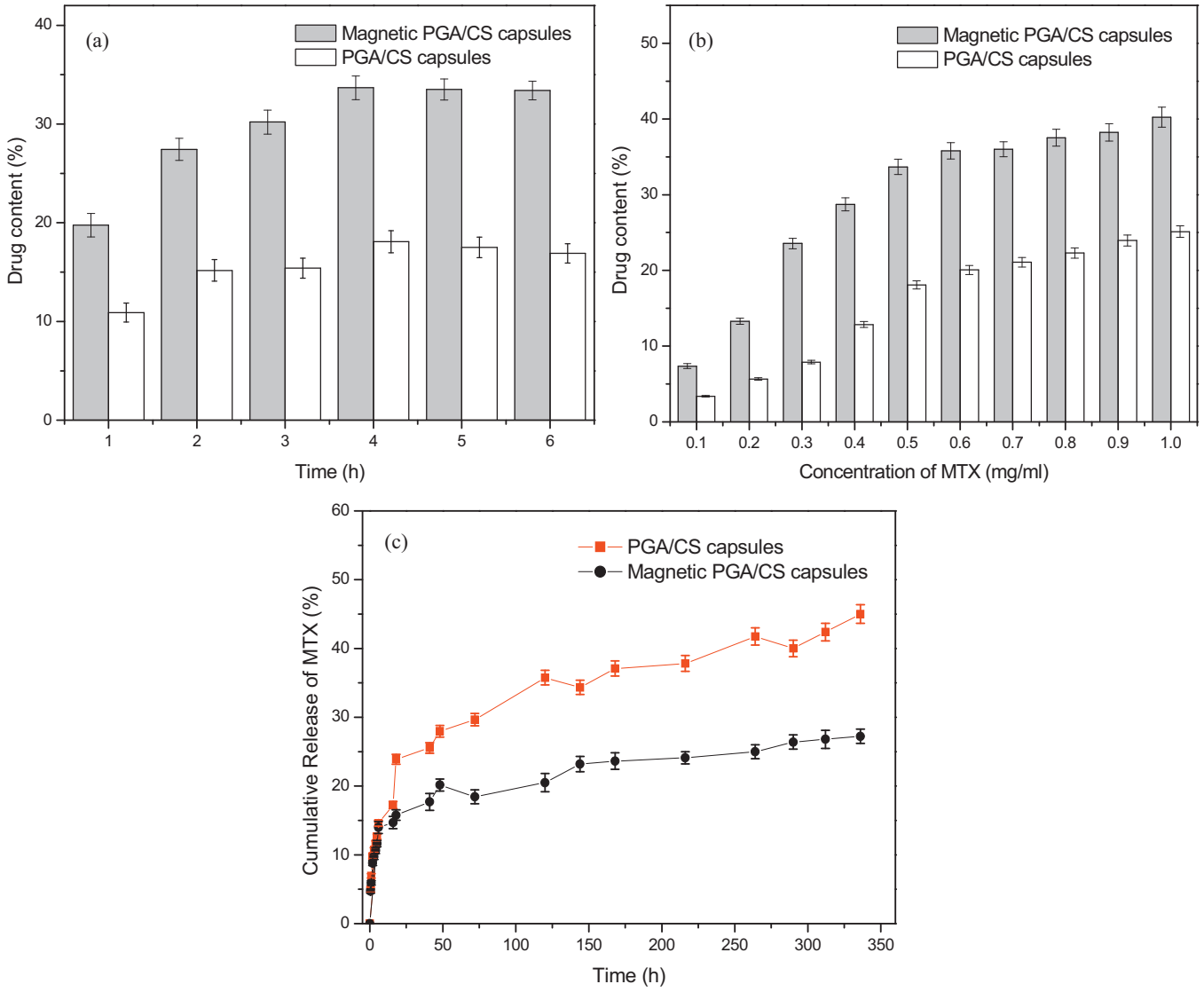

Fig. 6. MTX loading and release. MTX content of PGA/CS and magnetic PGA/CS microcapsules as a function of loading time (a) and initial MTX concentration (b). (c) Cumulative release curves of MTX from MTX-loaded PGA/CS and magnetic PGA/CS microcapsules.

Table 1
Fitted equations of cumulative release curves.

Samples	Kinetic model	Equation	Correlation coefficient
PGA/CS microcapsules	Zero-order	$Q = 0.17433 + 0.00237 \times t$	0.86774
	First-order	$\ln(1-Q) = -0.19285 - 0.00327 \times t$	0.90101
	Korsmeyer–Peppas	$\ln Q = -1.94512 + \mathbf{0.20477} \times \mathrm{Int}$	**0.99053**
	Baker–Lonsdale	$3/2[1-(1-Q)^{2/3}] - Q = 0.00597 + 0.00025 \times t$	**0.96888**
Magnetic PGA/CS microcapsules	Zero-order	$Q = 0.09893 + 0.00333 \times t$	0.9629
	First-order	$\ln(1-Q) = -0.10076 - 0.00426 \times t$	0.97531
	Korsmeyer–Peppas	$\ln Q = -2.6903 + \mathbf{0.35658} \times \mathrm{Int}$	**0.98928**
	Baker–Lonsdale	$3/2[1-(1-Q)^{2/3}] - Q = 0.00077 + 0.00028 \times t$	**0.99384**

microcapsules carried negative charge, the driving force for MTX absorption should be ascribed to electrostatic interaction, as discussed above. Moreover, the chance for contact between MTX and magnetic PGA/CS microcapsules was expected to be greatly elevated because of high specific surface area of nanoporous PGA/CS microcapsules and magnetic nanoparticles. The deposited MTX was in an aggregated or complexed form, rather than existing in its free state, which constrained the system so that the real concentration of the deposited substance within the interior of the magnetic microcapsule remained lower than in the bulk [42].

Therefore, the MTX loading capacity of magnetic PGA/CS microcapsules could be adjusted by loading time and MTX concentration. Obviously, the loading capability of magnetic PGA/CS microcapsules was superior to that of PGA/CS microcapsules. The Fe_3O_4 nanoparticles in the PGA/CS microcapsules played an important role in promoting the MTX absorption. In addition to the electrostatic interaction between PGA/CS microcapsules and MTX, the Fe_3O_4 nanoparticles provided an additional electrostatic interaction with MTX. Luo et al. also reported Fe_3O_4 nanoparticles in the cellulose microspheres could improve the absorption capacity and absorption rate of bovine serum albumin (BSA), they attributed this to the binding between BSA molecules and the orbitals of the Fe atom [27].

The release profiles of MTX from PGA/CS microcapsules and magnetic PGA/CS microcapsules were depicted in Fig. 6(c). For both PGA/CS microcapsules and magnetic PGA/CS microcapsules, the initial burst release was observed within 18 h, which might correspond to the release of drug on the surface of microcapsules. PGA/CS microcapsules showed sustained release behavior with cumulative release amount of 48.8% at 14 d. Compared with PGA/CS microcapsules, the MTX release from magnetic PGA/CS microcapsules further slowed down and reached equilibrium at about 14 d with a cumulative release amount of 29.2%. The incorporated positively charged MTX was strongly attracted to the negatively Fe_3O_4 nanoparticles and PGA chains, restricting the release.

For mathematical evaluations of the drug release process, the drug release kinetics obtained by fitting various standard release models and mathematical equations such as zero-, first-, Korsmeyer–Peppas and Baker–Lonsdale equation to the experimental data were characterized [43–47]. Simulated equations and correlation coefficients were calculated and compared in Table 1. The most suited being the one which best fitted the experimental results. It was clearly observed that MTX release from microcapsules was better described using Korsmeyer–Peppas and Baker–Lonsdale models where correlation coefficient was greater than 0.968 under all conditions than first-order and zero-order model with lesser values of correlation coefficient.

Korsmeyer–Peppas semi-empirical model was applied in order to better characterize the drug release behavior and understand the corresponding mechanism for the microcapsules studied.

$$\frac{Q}{Q_\infty} = kt^n$$

where Q/Q_∞ is the fraction of drug released at time t, k a constant comprising the structural and geometric characteristics of the tablet, and n the release exponent, is a parameter which depends on the release mechanism and is thus used to characterize it. For spherical tablet, the threshold of n value between Fickian and non-Fickian mechanism is 0.43. In particular, $n \leq 0.43$ corresponds to a Fickian diffusion release, whereas n between 0.43 and 0.85 indicates an anomalous non-Fickian transport [43].

Korsmeyer–Peppas semi-empirical model describes drug release from slabs, cylinders, and spheres [48]. In the current study, the model for spheres was used to describe the drug release behaviors of nanoporous PGA/CS microcapsules with a non-uniform drug distribution. The n value given in Table 1 for PGA/CS microcapsules and magnetic PGA/CS microcapsules was 0.20477 and 0.35658, indicating mechanism of MTX diffusion. Moreover, the drug release conformed well to the Baker–Lonsdale model with correlation coefficient of about 0.99, also indicating diffusion mechanism of drug release from PGA/CS microcapsules and magnetic PGA/CS microcapsules.

4. Conclusions

Magnetic PGA/CS microcapsules were prepared using an in situ synthesis of magnetic Fe_3O_4 nanoparticles in the presence of nanoporous PGA/CS microcapsules. PGA/CS microcapsules acted as microreactors for the absorption of iron ions and synthesis of magnetic Fe_3O_4 nanoparticles. Slice-and-view (FIB/SEM) was a useful tool to observe the inner microstructure of magnetic PGA/CS microcapsules. Fe_3O_4 nanoparticles with the average size of about 10 nm were homogeneously dispersed in the polymer matrix and adhered to the pore walls of the microcapsules. Depending initial concentration of iron ions, loading content of Fe_3O_4 nanoparticles and the magnetic properties of resultant magnetic PGA/CS microcapsules could be adjusted. The magnetic PGA/CS microcapsules showed high loading capacity of MTX under conditions of high loading time and drug concentration, which could be ascribed to spontaneous deposition of MTX induced by electrostatic interaction. MTX release from microcapsules took on a sustained release. Fitted equations of release curves corresponded to Korsmeyer–Peppas and Baker–Lonsdale models, revealing the diffusion mechanism. These results showed that PGA/CS microcapsules could serve as a kind of efficient drug delivery carrier in the future, because of the advantages of magnetic sensitivity, high drug loading and sustained release.

Acknowledgments

The work was supported by the National Natural Science Foundation of China (No. 51003055 and 51173101), the Science and Technology Commission of Shanghai Municipality (No. 11JC1404200), and the Innovation Program of Shanghai Municipal Education Commission (No. 11YZ06). Mr. Yuliang Chu and Bo

Lu from Instrumental Analysis Research Centre (Shanghai University) are acknowledged for their help in SEM and X-ray diffraction measurement.

References

[1] W.C. Yang, R. Xie, X.Q. Pang, X.J. Ju, L.Y. Chu, J. Membr. Sci. 321 (2008) 324.
[2] L.Y. Chu, S.H. Park, T. Yamaguchi, S. Nakao, Langmuir 18 (2002) 1856.
[3] C. Déjugnat, G.B. Sukhorukov, Langmuir 20 (2004) 7265.
[4] G. Ibarz, L. Dähne, E. Donath, H. Möhwald, Adv. Mater. 13 (2001) 1324.
[5] B. Zebli, A.S. Susha, G.B. Sukhorukov, A.L. Rogach, W.J. Parak, Langmuir 21 (2005) 4262.
[6] H.L. Guo, X.P. Zhao, J.P. Wang, J. Colloid Interface Sci. 284 (2005) 646.
[7] H.X. Liu, C.Y. Wang, Q.X. Gao, X.X. Liu, Z. Tong, Acta Biomater. 6 (2010) 275.
[8] H.X. Liu, C.Y. Wang, Q.X. Gao, X.X. Liu, Z. Tong, Mater. Lett. 63 (2009) 884.
[9] Y. Sun, Y.Y. Zheng, H.T. Ran, Y. Zhou, H.X. Shen, Y. Chen, H.R. Chen, Ti.M. Krupkac, A. Li, P. Li, Z.B. Wang, Z.G. Wang, Biomaterials 339 (2012) 5854.
[10] Z.J. Wei, C.Y. Wang, S.W. Zou, H. Liu, Z. Tong, Colloids Surf. A: Physicochem. Eng. Aspects 392 (2011) 116.
[11] E. Donath, G.B. Sukhorukov, F. Caruso, S.A. Davis, H. Möhwald, Angew. Chem. Int. Ed. 37 (1998) 2201.
[12] R.A. Caruso, A. Susha, F. Caruso, Chem. Mater. 13 (2001) 400.
[13] A.A. Antipov, G.B. Sukhorukov, Adv. Colloid Interface Sci. 111 (2004) 49.
[14] S. Ye, C. Wang, X. Liu, Z. Tong, J. Control. Release 106 (2005) 319.
[15] Z. Liang, C. Wang, Z. Tong, W. Ye, S. Ye, React. Funct. Polym. 63 (2005) 85.
[16] A.P. Johnston, C. Cortez, A.S. Angelatos, F. Caruso, Curr Opin, Colloid Interface Sci. 11 (2006) 203.
[17] D.G. Shchukin, I.L. Radtchenko, G.B. Sukhorukov, Mater. Lett. 57 (2003) 1743.
[18] F. Caruso, A.S. Susha, M. Giersig, H. Möhwald, Adv. Mater. 11 (1999) 950.
[19] D.G. Shchukin, I.L. Radtchenko, G.B. Sukhorukov, J. Phys. Chem. B 107 (2003) 86.
[20] S.F. Yan, S.Q. Rao, J. Zhu, Z.C. Wang, Y. Zhang, Y.R. Duan, X.S. Chen, J.B. Yin, Int. J. Pharm. 427 (2012) 443.
[21] K. Luo, J.B. Yin, Z.J. Song, L. Cui, B. Cao, X.S. Chen, Biomacromolecules 9 (2008) 2653.
[22] W.S. Choi, H.Y. Koo, J.H. Park, D.Y. Kim, J. Am. Chem. Soc. 127 (2005) 16136.
[23] S.H. Huang, D.H. Chen, J. Hazard. Mater. 163 (2009) 174.
[24] Z.Z. Dai, J.B. Yin, S.F. Yan, T. Cao, J. Ma, X.S. Chen, Polym. Int. 56 (2007) 1122.
[25] P. Li, A.M. Zhu, Q.L. Liu, Q.G. Zhang, Ind. Eng. Chem. Res. 47 (2008) 7700.
[26] S.X. Bi, X.Y. Wei, N. Li, Z.L. Lei, Mater. Lett. 62 (2008) 2963.
[27] X.G. Luo, S.L. Liu, J.P. Zhou, L.N. Zhang, J. Mater. Chem. 19 (2009) 3538.
[28] S.H. Xuan, Q.L. Fang, L.Y. Hao, W.Q. Jiang, X.L. Gong, Y. Hua, Z.Y. Chen, J. Colloid Interface Sci. 314 (2007) 502.
[29] A.C. Small, J.H. Johnston, J. Colloid Interface Sci. 331 (2009) 122.
[30] W. Zhang, S.Y. Jia, Q. Wu, S.H. Wu, J.Y. Ran, Y. Liu, J.Y. Hou, Mater. Sci. Eng. C 32 (2012) 381.
[31] P.K. Wallace, B. Arey, W.F. Mahaffee, Micron 42 (2011) 579.
[32] P.C. King, S.H. Zahiri, M. Jahedi, Acta Mater. 56 (2008) 5617.
[33] J.G. Deng, Y.X. Peng, C.L. He, X.P. Long, P. Li, A.S.C. Chan, Polym. Int. 52 (2003) 1182.
[34] Z.H. Zhou, J.M. Xue, J. Wang, H.S.O. Chan, T. Yu, J. Appl. Phys. 91 (2002) 6015.
[35] J.G. Zhang, S.Q. Xu, E. Kumacheva, J. Am. Chem. Soc. 126 (2004) 7908.
[36] C. Pham-Huu, N. Keller, C. Estournès, G. Ehret, J.M. Grenèche, M.J. Ledoux, Phys. Chem. Chem. Phys. 5 (2003) 3716.
[37] J.H. Beijnen, A. Bult, W.J.M. Underberg, Mitoxantrone Hydrochloride, 17, Academic Press, 1988, pp. 221.
[38] A. Wani, E. Muthuswamy, G.H.L. Savithra, G.Z. Mao, S. Brock, D. Oupický, Pharm. Res. 29 (2012) 2407.
[39] M. Enache, E. Volanschi, J. Pharm. Sci. 100 (2011) 558.
[40] C.Y. Gao, X.Y. Liu, J.C. Shen, H. Möhwald, Chem. Commun. 17 (2002) 1928.
[41] C.Y. Gao, E. Donath, H. Möhwald, J.C. Shen, Angew. Chem. Int. Ed. 41 (2002) 3789.
[42] S.Q. Ye, C.Y. Wang, X.X. Liu, Z. Tong, B.Y. Ren, F. Zeng, J. Control. Release 112 (2006) 79.
[43] M.L. Vuebaa, L.A. Carvalhob, F. Veigaa, J.J. Sousaa, M.E. Pinaa, Eur. J. Pharm. Biopharm. 58 (2004) 51.
[44] J. Dredán, R. Zelkó, I. Antal, E. Bihari, I. Rácz, Int. J. Pharm. 160 (1998) 257.
[45] A. Sood, R. Panchagnula, Int. J. Pharm. 175 (1998) 95.
[46] R.W. Korsmeyer, R. Gurnya, E. Doelkera, P. Buria, N.A. Peppas, Int. J. Pharm. 15 (1983) 25.
[47] J.B. Schwartz, A.P. Simonelli, W.I. Higuchi, J. Pharm. Sci. 57 (1968) 274.
[48] P.L. Ritger, N.A. Peppas, J. Control. Release 5 (1987) 37.